atmosphere

MDPI

Article

Atmospheric Aging of Organic Carbon and Polycyclic Aromatic Compounds Emitted from Residential Solid Fuel Combustion: Effects of Fuel Type and Combustion Temperature

Yuwei Liu [1,†], Yu Peng [1,†], Yanjie Lu [1] and Yingjun Chen [1,2,*]

[1] Shanghai Key Laboratory of Air Quality and Environmental Health, Department of Environmental Science and Engineering, Fudan University, Shanghai 200433, China; 22210740010@m.fudan.edu.cn (Y.L.); 23110740018@m.fudan.edu.cn (Y.P.); 25110740019@m.fudan.edu.cn (Y.L.)
[2] Shanghai Institute of Pollution Control and Ecological Security, Shanghai 200092, China
* Correspondence: yjchenfd@fudan.edu.cn
† These authors contributed equally to this work.

Abstract

Residential solid fuels are widely used for cooking and heating, but the atmospheric evolution of their particulate emissions remains insufficiently characterized. To address this gap, we constructed an integrated quartz-tube furnace–dilution–oxidation flow reactor (OFR) system for direct comparison of fresh and OFR-aged emissions across fuel types and combustion temperatures. Six biomass fuels and six coals were burned at 500 °C and 800 °C. Organic carbon (OC) subfractions and polycyclic aromatic compounds (PACs), including 16 parent polycyclic aromatic hydrocarbons (pPAHs) and 9 oxygenated polycyclic aromatic hydrocarbons (oPAHs), were quantified. In fresh emissions, increasing temperature reduced OC emission factors for both fuel types, whereas PAC emission factors increased for biomass but decreased for coal. OFR aging generally increased particulate OC and shifted OC toward less volatile or more thermally stable fractions. For coal burned at 500 °C, pPAHs decreased by 64%, whereas oPAHs increased by 127%. Although the overall quantitative structure–activity relationship (QSAR)-derived carcinogenicity indicator of PACs decreased by 46%, the oPAH contribution increased from 7% to 18%. These findings show that metrics based only on fresh emissions cannot fully capture the chemical evolution and toxicity-related implications of residential solid fuel emissions.

Keywords: residential solid fuel combustion; atmospheric aging; organic carbon; polycyclic aromatic compounds; oxidation flow reactor

Academic Editor: Jaroslaw Krzywanski

Received: 23 April 2026
Revised: 26 May 2026
Accepted: 1 June 2026
Published: 3 June 2026

1. Introduction

Residential solid fuels remain important energy sources for cooking and decentralized heating in many developing regions, and their combustion emissions are considered major sources of indoor and outdoor fine particulate matter (PM) as well as associated toxic organic pollutants [1–5]. Compared with utility boilers and industrial combustion systems, residential solid fuel combustion is typically characterized by lower combustion temperatures, unstable oxygen supply, and the absence of end-of-pipe pollution control; consequently, its emission factors for particulate matter, organic carbon, and aromatic pollutants are often higher [1–3]. In these emissions, particulate organic carbon (OC) is not only a major mass component of fine particulate matter but also an important determinant of particle volatility, hygroscopicity, and subsequent transformation potential. Polycyclic

aromatic compounds (PACs) and their derivatives, by contrast, continue to attract attention because of their carcinogenic, mutagenic, and oxidative stress effects [6–11]. Therefore, given the continued reliance on biomass and residential coal in many regions, clarifying the characteristics and atmospheric evolution of particulate organic emissions from residential solid fuel combustion is important for emission characterization, risk-informed control, and more complete evaluation of solid-fuel use.

Fuel type and combustion temperature are the two principal factors controlling the emission characteristics of residential solid fuels. Biomass is composed mainly of cellulose, hemicellulose, and lignin, whereas coal generally exhibits a higher degree of aromaticity and a more complex solid-phase structure; accordingly, the reaction pathways of different fuels during pyrolysis, cracking, and condensation differ fundamentally [12–16]. Previous studies have shown that low-temperature combustion generally favors the formation and retention of particulate OC. However, as combustion temperature increases, coal and biomass do not respond in the same way with respect to PAC emissions: parent polycyclic aromatic hydrocarbons (pPAHs) from coal combustion often decrease, whereas lignocellulosic biomass may exhibit increased pPAH emissions and enrichment of high-ring components [9,13]. At the same time, oxygenated polycyclic aromatic hydrocarbons (oPAHs) may be generated both directly during combustion and secondarily from parent PAHs during subsequent oxidation, and their relative contribution often varies with combustion conditions, precursor composition, and stove type [7–10]. These findings indicate that focusing solely on bulk emission levels is insufficient to reveal the true environmental differences among fuels and combustion conditions, and that greater attention should be paid to compositional structure and its controlling factors.

Fresh emissions do not remain chemically and physically static after release into the atmosphere; instead, they can undergo atmospheric aging and continue to evolve during transport. Atmospheric aging involves processes such as oxidation, condensation, evaporation, and gas–particle partitioning, which can further modify particle mass, composition, volatility, and oxidation state. Numerous studies have shown that biomass-burning organic aerosols may undergo substantial oxygenation, reduced volatility, and secondary organic aerosol formation following photochemical oxidation, thereby altering particle mass and composition [17–25]. Under dark-aging or chamber conditions, smoke particles may also undergo sustained oxidation and condensation, driving particulate organic matter toward lower volatility and a higher oxidation state [19,20]. For PACs, low- and medium-ring parent PAHs are more susceptible to gas-phase or particle-phase oxidation, whereas high-ring PAHs, owing to their greater particle-phase partitioning, often account for a larger fraction of the residual particulate phase. Meanwhile, oxygenated aromatic compounds may be retained or even formed secondarily during aging [21,26–29]. Recent studies further suggest that oPAHs are not only closely associated with particle oxidative potential but may also participate in the formation of low-maturity elemental carbon (EC) and brown carbon (BrC), thereby influencing the optical properties and health effects of particles [30,31]. Therefore, evaluations of residential solid-fuel emissions should not be confined to fresh emissions, but should incorporate post-emission atmospheric transformation into the same analytical framework.

Although considerable progress has been made, several clear gaps remain in the current understanding. First, existing studies have largely focused on actual stove emissions or a single fuel type, making it difficult to isolate, within a unified framework, the independent effects of fuel type and combustion conditions on the evolution of particulate organic components. Second, many studies have focused primarily on changes in PM or total organic aerosol, with insufficient attention paid to the coupled evolution of OC subfractions and pPAHs/oPAHs; consequently, the linkage between carbonaceous

restructuring and the formation of oxidized aromatic products remains poorly characterized. In addition, discussion of combustion-temperature effects has often remained limited to primary emissions, whereas systematic comparisons of the subsequent atmospheric evolution of emissions under different combustion intensities are still lacking. As a result, evaluation of the environmental performance and risk implications of residential solid fuels may remain incomplete if it relies only on fresh-emission indicators. If the benefits of fuel substitution or combustion optimization are judged solely on the basis of reductions in initial PM or parent PAHs, post-emission shifts in oPAHs, pyrolyzed carbon (PyC), or other oxidized components can be overlooked, together with their toxicity-related contribution profiles [9,10,21,27,31].

Against this background, the present study focuses on the atmospheric evolution of particulate organic components emitted from residential solid fuel combustion during simulated aging. An integrated combustion–dilution–oxidation flow reactor (OFR) system was constructed to directly compare fresh and OFR-aged particles under a unified experimental framework. Six biomass fuels and six coals were burned in a quartz tube furnace at two representative ignition temperatures, 500 °C and 800 °C, to examine how fuel type and combustion temperature affect initial emissions and aging-induced compositional changes. Particulate OC and its subfractions (OC1–OC4 and PyC), together with PACs including 16 pPAHs and 9 oPAHs, were quantified. On this basis, the potential carcinogenicity indicators of target PACs were further evaluated using a quantitative structure–activity relationship (QSAR) model [32], and the implications of different fuel–temperature combinations for residential solid fuel utilization and low-emission control assessment were discussed. This study aims to clarify, within a unified experimental system, how fuel type, combustion temperature, and post-emission transformation jointly influence the evolution of particulate organic components, thereby providing a more complete basis for evaluating emissions from residential solid fuels.

2. Materials and Methods

2.1. Combustion–Dilution–Aging–Sampling System

In this study, an integrated combustion–dilution–aging–sampling system was employed. This system was developed based on established experimental protocols previously developed by our group [13,33] and was used to simulate, within a unified experimental framework, the generation of particulate emissions from residential solid fuel combustion and their subsequent atmospheric aging. The system mainly consisted of a quartz tube furnace, a flue-gas dilution unit, a potential aerosol mass oxidation flow reactor (PAM-OFR, hereinafter referred to as the OFR), and a filter sampling unit.

The flue gas generated during combustion was first mixed with clean air for dilution, and the CO_2 and CO concentrations before and after dilution were monitored using a gas analyzer to calculate and control the dilution ratio. Because the dilution process itself can affect gas–particle partitioning and thereby influence the measurement results [34,35], the dilution ratio was fixed at 1:15 for all experiments in this study. One portion of the diluted flue gas was collected directly as the fresh-emission sample (Fresh), representing the initial particulate emissions collected immediately after combustion and dilution. The other portion was introduced into the OFR and then collected as the OFR-aged sample (Aged), representing particles obtained after simulated atmospheric aging of the fresh emissions. Both Fresh and Aged samples were collected as total particulate matter on 90 mm quartz fiber filters.

The aging experiments were conducted using a PAM-OFR system (Aerodyne Research Inc., Billerica, MA, USA) operated in the OFR254 mode, in which OH radicals were generated through 254 nm UV irradiation of an O_3–H_2O system. The total flow through the

reactor was maintained at 17 L/min, corresponding to a residence time of approximately 116.7 s and an equivalent atmospheric aging time of approximately 3–5 d [36,37]. Temperature, relative humidity, and the outlet O_3 concentration were continuously monitored during the experiments, and the calculation methods for OH exposure and equivalent aging time are described in the Supplementary File. After each experiment, the reactor and sampling lines were purged with high-flow zero air to minimize the influence of residual background.

2.2. Fuel Sample Preparation and Combustion Experiment Design

A total of 12 typical residential solid fuels were selected in this study, including six biomass fuels and six bituminous coal samples. The biomass fuels included both crop residues and wood, namely rice straw, wheat straw, corn straw, poplar wood, willow wood, and pine wood, whereas the coal samples spanned a range of volatile matter contents, with dry ash-free volatile matter ranging from 20% to 35.5%.

Biomass samples were naturally air-dried, cleaned of impurities, and cut into pieces approximately 2–3 cm in length, whereas coal samples were ground and passed through a 200-mesh sieve to ensure reproducible combustion conditions. Before each experiment, the tube furnace was preheated to the target ignition temperature. Two ignition temperatures, 500 °C and 800 °C, were used to represent low initial combustion temperature (LIC) and high initial combustion temperature (HIC), respectively. Once the furnace temperature had stabilized, 1.0 g of pretreated fuel was introduced into the combustion zone and burned under a clean compressed air flow of 5 L/min.

These two ignition temperatures were used to represent typical combustion states of different intensities during residential solid fuel combustion: 500 °C corresponds to relatively low-intensity, less complete combustion, whereas 800 °C corresponds to relatively high-intensity, more complete combustion [12,13,33]. For each fuel at each temperature, both Fresh and Aged samples were collected, and two replicate experiments were conducted.

2.3. Chemical Analysis

2.3.1. Carbonaceous Component Analysis

Carbonaceous components in quartz fiber filter samples were determined using a modified thermal/optical reflectance method (TOR, DRI Model 2001A carbon analyzer, Atmoslytic Inc., Calabasas, CA, USA). During analysis, filter punches were first heated stepwise to 120, 250, 450, and 550 °C under a pure He atmosphere, corresponding to the release of OC1, OC2, OC3, and OC4, respectively. The atmosphere was then switched to an oxidizing gas mixture containing 2% O_2 and 98% He, and heating was continued to determine the more thermally stable carbon fractions. PyC was defined as the amount of pyrolyzed carbon released before the laser reflectance signal returned to its initial value, and total organic carbon (OC) was calculated as the sum of OC1, OC2, OC3, OC4, and PyC. In general, a higher release temperature indicates lower volatility or greater thermal stability of the corresponding fraction. The organic carbon emission factor (EF_{OC}) for each sample was calculated using the carbon mass balance method.

2.3.2. PACs Analysis

Particulate-phase polycyclic aromatic compounds (PACs) were analyzed using thermal desorption–gas chromatography/mass spectrometry (TD-GC/MS; OPTIC-4, GL Sciences B.V., Eindhoven, The Netherlands; TRACE 1300 gas chromatograph and ISQ 7000 single quadrupole mass spectrometer, Thermo Fisher Scientific, Waltham, MA, USA) in selected ion monitoring (SIM) mode. The target compounds included 16 parent polycyclic aromatic hydrocarbons (pPAHs) and 9 oxygenated polycyclic aromatic hydrocarbons

(oPAHs). For subsequent data analysis, pPAHs were further grouped into the 2–4 rings and 5–6 rings categories, whereas oPAHs were grouped into anthraquinone-like (ANTQ), benz[a]anthrone-like (BANO), and Other categories. All target compounds were quantified using the external standard method, with calibration concentrations ranging from 2 to 200 pg/μL and correlation coefficients (R^2) of no less than 0.99. This analytical method is consistent with that used in our group's previous studies on PAC emissions [12].

2.3.3. Evaluation of Potential Carcinogenicity

To evaluate compound-based potential carcinogenicity indicators for the target particle-bound PACs, two approaches were adopted in this study. First, the measured pPAHs and oPAHs were characterized using quantitative structure–activity relationship (QSAR)-derived carcinogenicity parameters provided by ADMETlab 2.0 [32]. Second, the 16 pPAHs were also evaluated using the benzo[a]pyrene equivalent (BaPeq) method for comparison [38].

2.4. Calculation of Emission Factors and Quality Control

The emission factors (EFs) of all target components were calculated using the carbon mass balance method and expressed as the mass of target pollutants emitted per unit mass of fuel burned. This method assumes that the carbon in the consumed fuel is mainly emitted as CO_2, CO, and particle-phase carbonaceous species, and has been widely used in combustion emission studies [12,33,39]. In this study, the measured mass of each target compound on the filter punch was first converted to the total mass collected on the whole effective filter area according to the ratio of the punched area to the effective sampling area. The total collected mass was then scaled by the sampling flow, dilution flow, flue-gas flow entering the dilution chamber, and the actual mass of fuel consumed to obtain fuel-mass-based EFs. Detailed equations and parameter definitions are provided in Text S6. The unit for OC was g/kg fuel, whereas the unit for PACs was mg/kg fuel.

To improve the reliability of EF calculation, potential uncertainties associated with fuel heterogeneity, combustion repeatability, flow-rate control, dilution-ratio determination, filter-punch representativeness, blank correction, and instrumental analysis were controlled through standardized experimental and quality assurance/quality control (QA/QC) procedures. Specifically, all experiments were conducted under fixed airflow and dilution conditions, duplicate combustion experiments were performed for each fuel–temperature–aging combination, and blank correction and replicate analyses were included in the analytical procedure.

All quartz fiber filters were prebaked at 450 °C for 4 h before sampling to remove background organic contamination. After sampling, the filters were sealed immediately and stored at −18 °C until analysis. During PACs analysis, deuterated standards were used to assess recoveries, and the recoveries of all target compounds were within acceptable ranges. Procedural blanks and filter blanks were both used for background correction, and the relative deviations of replicate experiments were below 10%, indicating good repeatability of the experimental method.

3. Results and Discussion

3.1. Emission Levels and Compositional Characteristics of OC in Fresh Emissions

Figure 1 shows the average emission factors (EF_{OC}) and compositional characteristics of particulate organic carbon (OC) in fresh emissions from biomass and coal fuels. In Figure 1, the bars represent OC emission factors, with the blue bars indicating the emission factors under LIC conditions and the red bars indicating those under HIC conditions. The double-ring charts show the relative contributions of OC1+2, OC3+4, and PyC under LIC

and HIC conditions. In the double-ring charts, the inner and outer rings correspond to LIC and HIC, respectively, and different colors denote different OC fractions. The levels of particulate OC differed markedly across fuel types and combustion temperatures. At 500 °C, the average EF_{OC} values for biomass and coal were 9.16 ± 8.55 and 6.14 ± 2.22 g/kg fuel, respectively; when the temperature was increased to 800 °C, they decreased to 5.71 ± 5.62 and 0.08 ± 0.03 g/kg fuel, respectively. These values generally fell within the ranges reported in previous laboratory simulations and residential combustion studies [1,6,15,40]. Overall, increasing temperature significantly reduced particulate OC emissions, with a much steeper decline observed for coal under high-temperature conditions. This pattern suggests a fuel-dependent temperature response: coal-derived volatile and semi-volatile organic products were more effectively removed under high-temperature conditions, whereas biomass-derived organics, especially from woody fuels, were more readily retained in the particle phase. Across both temperatures, biomass consistently exhibited higher EF_{OC} values than coal.

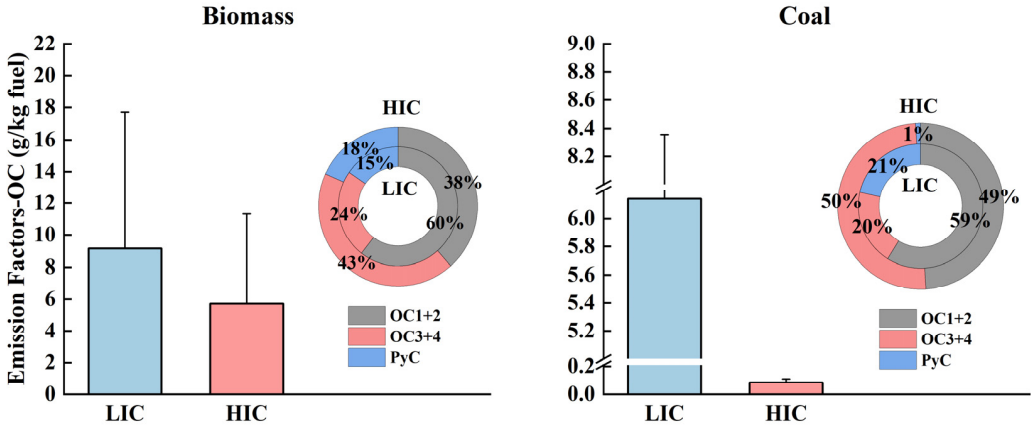

Figure 1. OC emission factors and compositional characteristics of biomass and coal in fresh emissions under low-temperature (LIC) and high-temperature (HIC) combustion conditions. In the double-ring charts, the inner and outer rings represent LIC and HIC, respectively. Percentages are rounded to the nearest whole number; therefore, the displayed values may not sum exactly to 100%.

Further differentiation of biomass types showed that the average EF_{OC} values for wood at 500 °C and 800 °C were 11.92 ± 11.44 and 9.52 ± 5.85 g/kg fuel, respectively, both of which were higher than those for straw, at 6.39 ± 5.39 and 1.89 ± 1.08 g/kg fuel, respectively. Under 800 °C, coal samples as a whole remained at extremely low levels, with only minor differences among individual coal samples. These results indicate that woody fuels still maintained relatively high particulate OC emissions under high-temperature conditions, whereas particulate OC from coal was much more strongly suppressed at high temperature. This contrast is consistent with differences in fuel structure and devolatilization behavior: lignocellulosic biomass generally releases more condensable organic vapors during pyrolysis, whereas coal-derived organic products are more readily reduced by cracking and oxidation as combustion temperature increases [1,12].

The OC compositional profiles further indicate that increasing temperature changed not only the total amount of OC emitted but also the thermal stability of the emitted carbonaceous material. At 500 °C, OC emissions from both biomass and coal were dominated by OC1+2, with average contributions of 60% and 59%, respectively. OC3+4 accounted for 24% and 20%, respectively, whereas PyC accounted for 15% and 21%, respectively. At 800 °C, the compositions of both fuel groups shifted toward more thermally stable fractions: in biomass, OC1+2 decreased to 38%, OC3+4 increased to 43%, and PyC accounted for 18%; in coal, OC1+2 and OC3+4 accounted for 49% and 50%, respectively, whereas PyC

decreased to 1%. Wood still exhibited relatively high OC emissions at 800 °C, accompanied by relatively high fractions of OC3+4 and PyC; by contrast, particulate OC from coal at 800 °C was nearly completely suppressed. Overall, increasing temperature promoted a shift in fresh emissions from low-temperature-evolving OC toward more thermally stable fractions, which is consistent with the understanding that lignin more readily forms aromatized and charred products, whereas organic matter in coal more readily cracks and is further oxidized at high temperature [1,12]. From the perspective of residential solid fuel utilization, these results suggest that reducing OC emissions cannot rely only on increasing combustion temperature because fuel-dependent differences in carbon release and retention remain important.

3.2. Emission Levels and Compositional Characteristics of PACs in Fresh Emissions

In addition to OC, the emission behavior of polycyclic aromatic compounds (PACs) also varied significantly with fuel type and combustion temperature (Figure 2). In Figure 2, the stacked bars represent the emission factors of pPAHs and oPAHs, with the blue portions indicating pPAH emission factors and the green portions indicating oPAH emission factors. The ring charts show the relative contributions of pPAH ring groups and oPAH categories under LIC and HIC conditions, with the inner and outer rings corresponding to LIC and HIC, respectively. At 500 °C, the average emission factors (EF_{PACs}) of particulate PACs (pPAHs + oPAHs) from biomass and coal combustion were 34.32 ± 16.87 and 308.49 ± 155.37 mg/kg fuel, respectively; when the temperature was increased to 800 °C, the value for biomass increased to 62.93 ± 31.72 mg/kg fuel, whereas that for coal decreased to 95.27 ± 52.38 mg/kg fuel. These values generally fell within the ranges reported in previous laboratory simulations and residential combustion studies [6–8,13]. These opposite temperature responses indicate that PAC emissions were governed not only by combustion intensity but also by fuel-specific chemical structure and competing formation, cracking, and oxidation pathways.

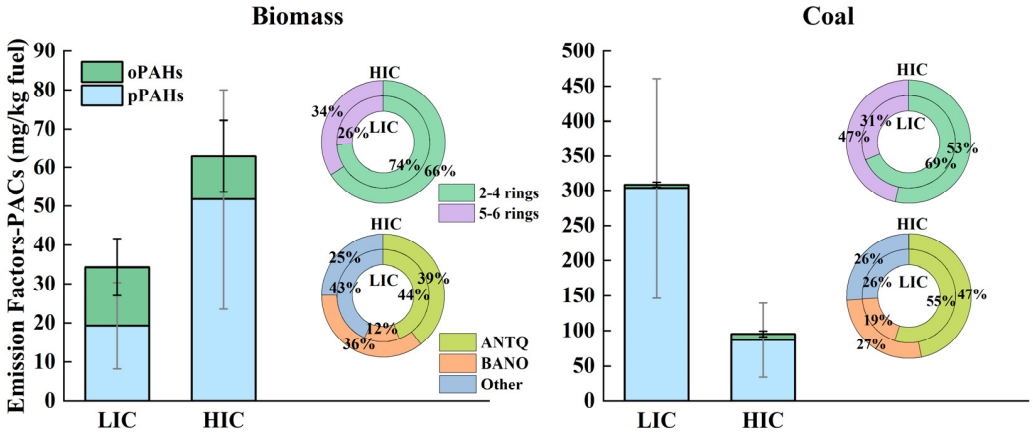

Figure 2. PAC emission factors and compositional characteristics of biomass and coal in fresh emissions under low-temperature (LIC) and high-temperature (HIC) combustion conditions. In the ring charts, the inner and outer rings represent LIC and HIC, respectively. Percentages are rounded to the nearest whole number; therefore, the displayed values may not sum exactly to 100%.

Biomass and coal did not respond in the same way to increasing temperature. In biomass, pPAHs increased from 19.35 ± 11.03 to 51.77 ± 28.23 mg/kg fuel, whereas oPAHs decreased from 14.97 ± 7.27 to 11.16 ± 9.33 mg/kg fuel. In coal, by contrast, pPAHs decreased from 303.58 ± 157.03 to 86.93 ± 52.49 mg/kg fuel, whereas oPAHs increased from 4.91 ± 3.58 to 8.35 ± 4.08 mg/kg fuel. Thus, increasing temperature enhanced particulate pPAH emissions from biomass but strongly reduced those from coal, while oPAHs showed

a smaller and opposite response between the two fuel groups. Correspondingly, at 500 °C, pPAHs emitted from both biomass and coal were dominated by the 2–4 rings group, accounting for 74% and 69%, respectively. When the temperature was increased to 800 °C, the fraction of the 2–4 rings group in biomass decreased to 66%, and that in coal further decreased to 53%, with the fraction of the 5–6 rings group correspondingly increasing to 34% and 47%, respectively. This pattern is consistent with previous findings that higher combustion temperature can promote aromatic growth and high-ring PAH formation in biomass burning, whereas in coal combustion, it is associated with enhanced cracking and oxidation of particle-bound parent PAHs [9,13].

The changes in oPAHs exhibited a stronger dependence on source type. At 500 °C, ANTQ and Other accounted for similar proportions in biomass emissions, at 44% and 43%, respectively, whereas BANO accounted for 12%. When the temperature was increased to 800 °C, the fraction of BANO increased to 36%, whereas that of Other decreased to 25%. oPAHs emitted from coal were dominated by ANTQ at both temperatures, accounting for 55% and 47% at 500 °C and 800 °C, respectively, whereas the fraction of BANO increased from 19% to 27%. This indicates that although the total amount of oPAHs from biomass decreased slightly with increasing temperature, the internal composition shifted from a co-dominance of ANTQ and Other toward an enhanced contribution of BANO. In coal, by contrast, the total pPAHs decreased, whereas the relative contribution of oPAHs, especially BANO, within total oPAHs increased. Previous studies have shown that oPAH emissions are influenced not only by the abundance of parent PAHs but also by combustion temperature, oxidation level, and the composition of aromatic precursors in the fuel [7,9,12].

Within biomass, the emission factors of pPAHs from wood at 500 °C and 800 °C were 24.53 ± 13.48 and 69.45 ± 17.18 mg/kg fuel, respectively, both higher than those from straw, at 14.17 ± 7.54 and 34.09 ± 22.31 mg/kg fuel, respectively. The oPAHs from wood were slightly lower than those from straw at 500 °C, but became higher than those from straw at 800 °C. For biomass, the higher PAC emissions from wood than from straw, together with the increased contribution of 5–6 ring pPAHs at 800 °C, suggest that high-temperature combustion favored aromatic growth and the formation of less volatile parent PAHs in lignin-rich fuels. This interpretation is consistent with previous findings that lignin is more conducive to aromatic compound formation than cellulose and hemicellulose [12,41]. Coal showed a different response: high temperature greatly reduced particulate pPAHs but increased oPAHs, indicating that parent-compound depletion and oxygenated-product enrichment occurred simultaneously under HIC conditions [9,13]. Therefore, evaluating combustion optimization only by reductions in total particulate matter or total PACs can overlook shifts in PAC composition, especially the enrichment of high-ring pPAHs or oxygenated aromatic products.

3.3. Effects of Atmospheric Aging on Combustion-Emitted OC

As shown in Figure 3, particulate OC emitted from biomass and coal under both low- and high-temperature combustion conditions generally increased after OFR-simulated aging, although the magnitude of the increase varied with fuel type and combustion temperature. In Figure 3, panels a and b show the OC aging results under LIC and HIC conditions, respectively; within each panel, the left and right subplots correspond to biomass and coal. The boxplots show the distributions of OC emission factors in Fresh and Aged samples; Δ denotes $EF_{Aged} - EF_{Fresh}$, and the percentage indicates the relative change from the Fresh value to the Aged value. The double-ring charts show the relative contributions of OC1+2, OC3+4, and PyC, with the inner and outer rings representing Fresh and Aged samples, respectively. At 500 °C, the aged EF_{OC} of biomass was 10.37 ± 9.10 g/kg fuel, with OC1+2, OC3+4, and PyC accounting for 42%, 28%, and

29%, respectively; the corresponding value for coal was 7.58 ± 2.72 g/kg fuel, with these three fractions accounting for 47%, 27%, and 26%, respectively. Compared with fresh emissions, OC emissions from biomass and coal at 500 °C increased from 9.16 ± 8.55 to 10.37 ± 9.10 g/kg fuel and from 6.14 ± 2.22 to 7.58 ± 2.72 g/kg fuel, respectively, corresponding to increases of 13% and 23% and ΔEFOC values of 1.22 and 1.44 g/kg fuel. The increase for coal reached statistical significance (p = 0.001), whereas that for biomass was only marginally significant (p = 0.062). This increase is consistent with the continued formation or condensation of lower-volatility organic material during aging, which is more evident for emissions generated under lower-temperature combustion conditions [19,20,23,42,43].

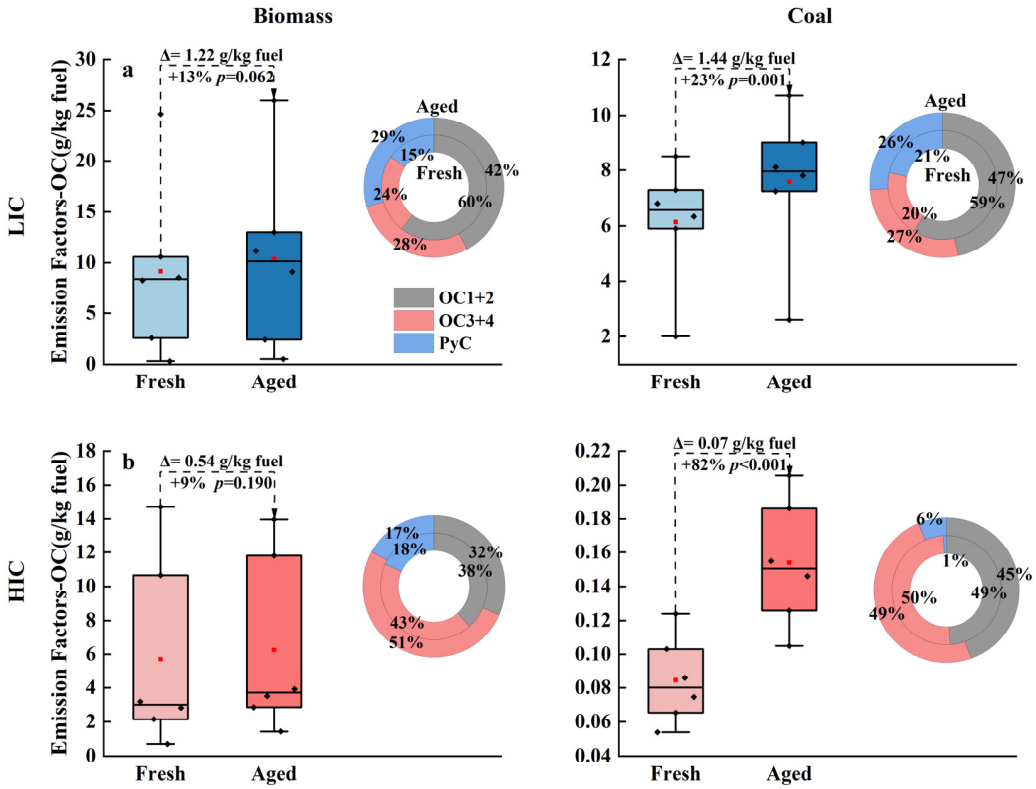

Figure 3. Changes in particulate OC from biomass and coal before and after atmospheric aging under (**a**) low-temperature combustion (LIC) and (**b**) high-temperature combustion (HIC) conditions. In each panel, the left and right subplots correspond to biomass and coal, respectively. In the double-ring charts, the inner and outer rings represent Fresh and Aged samples, respectively. Black symbols represent individual fuel samples, and red squares indicate group means. Percentages are rounded to the nearest whole number; therefore, the displayed values may not sum exactly to 100%.

At 800 °C, the aging response of particulate OC was markedly weaker. After aging, the EF_{OC} of biomass was 6.25 ± 5.26 g/kg fuel, with OC1+2, OC3+4, and PyC accounting for 32%, 51%, and 17%, respectively; for coal, the value was 0.15 ± 0.04 g/kg fuel, with the corresponding fractions accounting for 45%, 49%, and 6%, respectively. Compared with fresh emissions, OC emissions from biomass and coal under high-temperature conditions increased from 5.71 ± 5.62 to 6.25 ± 5.26 g/kg fuel and from 0.08 ± 0.03 to 0.15 ± 0.04 g/kg fuel, respectively, corresponding to increases of 9% and 82% and ΔEFOC values of 0.54 and 0.07 g/kg fuel. Although coal exhibited a larger relative increase at 800 °C, its fresh-emission OC level was extremely low, and therefore, the absolute contribution of aged coal-derived OC remained limited. Biomass, by contrast, maintained relatively high OC emissions at high temperature, but the absolute difference between fresh and aged samples was much smaller than that observed at 500 °C.

In addition to changes in total OC, atmospheric aging also altered the distribution of OC subfractions. At 500 °C, OC1+2 in biomass decreased from 60% to 42%, whereas OC3+4 and PyC increased from 24% and 15% to 28% and 29%, respectively. In coal, OC1+2 decreased from 59% to 47%, whereas OC3+4 and PyC increased from 20% and 21% to 27% and 26%, respectively. This indicates that the additional particulate OC formed after aging under low-temperature combustion conditions was not primarily expressed as a simple accumulation of low-temperature fractions but instead was more closely associated with increased proportions of mid- to high-temperature fractions and PyC. Previous studies have shown that biomass smoke particles can continue to undergo oxidation and secondary condensation during aging, driving organic components toward lower volatility and greater thermal stability [19,20,23,24,42].

At 800 °C, compositional changes were still observed, but they exhibited characteristics different from those under low-temperature conditions. In biomass, OC1+2 decreased from 38% to 32%, OC3+4 increased from 43% to 51%, whereas PyC decreased only slightly from 18% to 17%. Notably, the increase in PyC was much more pronounced at 500 °C, especially for biomass, for which it rose from 15% to 29%. Previous studies have shown that an increase in PyC usually corresponds to the enrichment of relatively heat-resistant and more highly oxidized carbonaceous fractions in the particulate phase, and that oPAHs may also participate in the formation of low-maturity EC and BrC [30]. Therefore, aging not only altered the emission level of particulate OC but was also accompanied by changes in the distribution of carbonaceous fractions. This also suggests that evaluations based solely on fresh OC emissions cannot fully reflect the subsequent chemical evolution of carbonaceous particles under different combustion conditions.

3.4. Effects of Atmospheric Aging on Combustion-Emitted PACs and Their Potential Risks

As shown in Figure 4, after atmospheric aging, particulate PACs emitted from biomass and coal under both low- and high-temperature combustion conditions generally exhibited a decline in pPAHs, whereas the direction and magnitude of changes in oPAHs remained jointly governed by fuel type and combustion temperature. In Figure 4, rows a and b present the pPAH aging results, with row a showing biomass and row b showing coal, whereas rows c and d present the oPAH aging results, with row c showing biomass and row d showing coal. Within each row, the left and right subplots correspond to LIC and HIC conditions, respectively. The boxplots show the emission-factor distributions of pPAHs and oPAHs in Fresh and Aged samples; Δ denotes $EF_{Aged} - EF_{Fresh}$, and the percentage indicates the relative change from the Fresh value to the Aged value. The double-ring charts show the compositional changes in pPAH ring groups and oPAH categories before and after aging. At 500 °C, in biomass, EF_{pPAHs} decreased from 19.35 ± 11.03 to 14.69 ± 6.46 mg/kg fuel, a reduction of 24%, with ΔEF_{pPAHs} of −4.66 mg/kg fuel ($p = 0.217$). EF_{oPAHs} increased from 14.97 ± 7.27 to 16.50 ± 7.29 mg/kg fuel, an increase of 10%, with ΔEF_{oPAHs} of 1.53 mg/kg fuel ($p = 0.501$). The changes in coal were more pronounced: EF_{pPAHs} decreased from 303.58 ± 157.03 to 110.79 ± 85.53 mg/kg fuel, a reduction of 64%, with ΔEF_{pPAHs} of −192.79 mg/kg fuel ($p = 0.043$), whereas EF_{oPAHs} increased from 4.91 ± 3.58 to 11.16 ± 1.67 mg/kg fuel, an increase of 127%, with ΔEF_{oPAHs} of 6.25 mg/kg fuel ($p = 0.076$). This opposite response suggests that low-temperature coal emissions contained abundant particle-bound parent PAHs that were susceptible to aging-driven loss, while oxygenated derivatives were concurrently formed or retained during the OFR aging process.

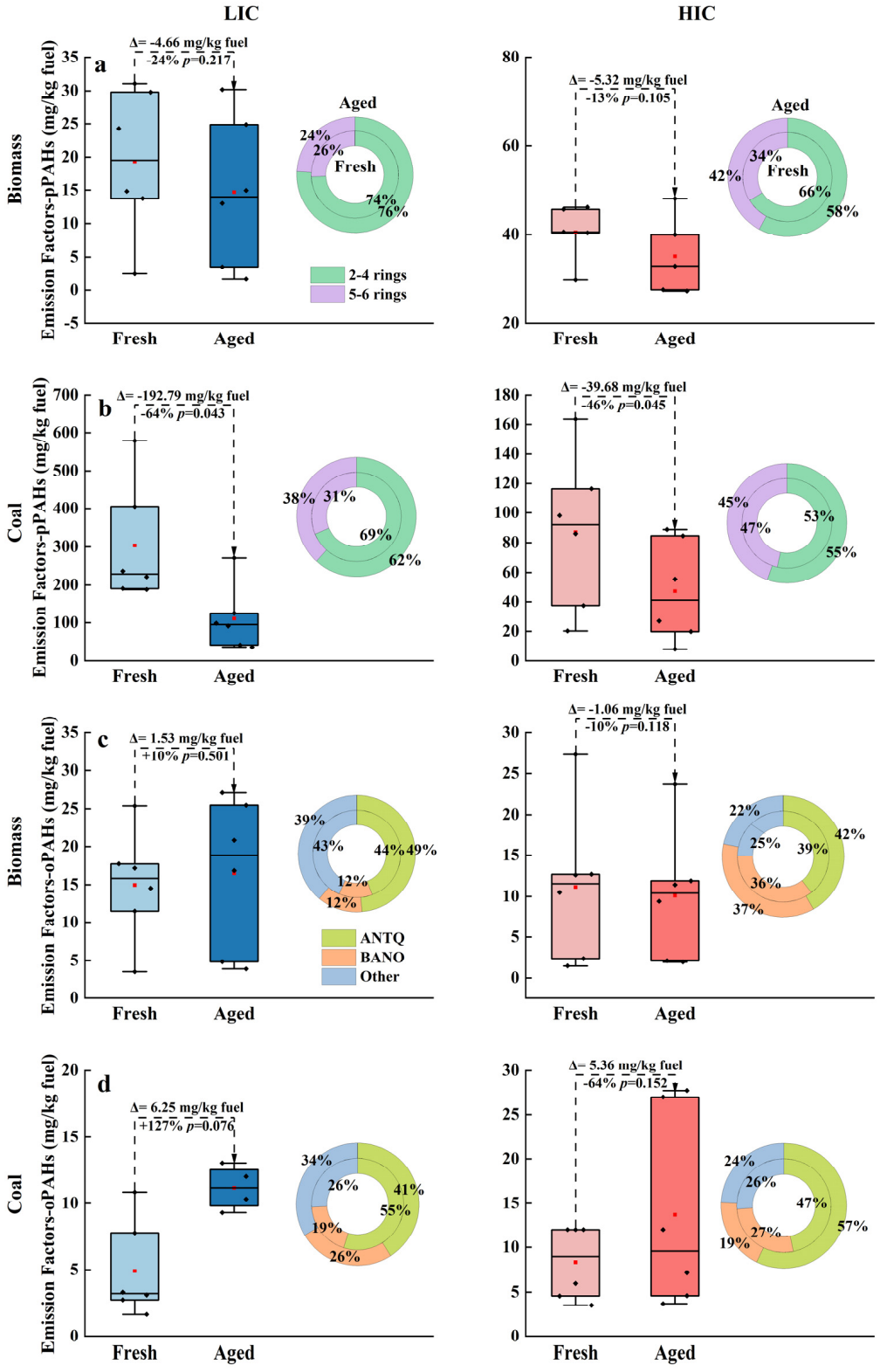

Figure 4. Changes in particulate pPAHs and oPAHs from biomass and coal before and after atmospheric aging under low-temperature (LIC) and high-temperature (HIC) combustion conditions: (**a**) pPAHs from biomass; (**b**) pPAHs from coal; (**c**) oPAHs from biomass; (**d**) oPAHs from coal. In each subfigure, the left and right subplots correspond to LIC and HIC, respectively. In the double-ring charts, the inner and outer rings represent Fresh and Aged samples, respectively. Black symbols represent individual fuel samples, and red squares indicate group means. Percentages are rounded to the nearest whole number; therefore, the displayed values may not sum exactly to 100%.

At 800 °C, the differences between biomass and coal became even more apparent. In biomass, EF_{pPAHs} decreased from 40.49 ± 6.55 to 35.17 ± 8.85 mg/kg fuel, a reduction of 13%, with ΔEF_{pPAHs} of −5.32 mg/kg fuel (p = 0.105). EF_{oPAHs} decreased from 11.16 ± 9.33 to 10.10 ± 9.71 mg/kg fuel, a reduction of 9%, with ΔEF_{oPAHs} of −1.06 mg/kg fuel (p = 0.118). By contrast, coal at 800 °C still showed decreasing pPAHs but increasing oPAHs: EF_{pPAHs} decreased from 86.93 ± 52.49 to 47.25 ± 35.02 mg/kg fuel, a reduction of 46%, with ΔEF_{pPAHs} of −39.68 mg/kg fuel (p = 0.045), whereas EF_{oPAHs} increased from 8.35 ± 4.08 to 13.70 ± 8.16 mg/kg fuel, an increase of 64%, with ΔEF_{oPAHs} of 5.35 mg/kg fuel (p = 0.152). These results indicate that coal emissions were more prone to aging-induced increases in oPAHs under both combustion temperatures, whereas high-temperature biomass showed relatively smaller changes in total PAC emissions but still retained clear compositional differences after aging.

Compositional changes indicate that aging did not reduce all PAC classes uniformly but instead involved the coexistence of parent-compound consumption and oxidative derivative restructuring. This behavior is consistent with the different aging reactivities of PAC groups: lower-ring parent PAHs are generally more reactive toward oxidation, whereas some higher-ring species and oxygenated derivatives can be relatively retained in the particle phase or formed through secondary pathways. At 500 °C, in biomass, the proportion of the 2–4 rings group within pPAHs increased from 74% to 76%, whereas that of the 5–6 rings group decreased from 26% to 24%. In coal, the corresponding values changed from 69% and 31% to 62% and 38%, respectively. At 800 °C, in biomass, the 2–4 rings group decreased from 66% to 58%, whereas the 5–6 rings group increased from 34% to 42%; in coal, the 5–6 rings fraction remained high after aging. At the same time, in biomass, the proportion of BANO increased from 36% to 37%, whereas in coal, the proportion of ANTQ increased from 47% to 57%, indicating that the restructuring of oPAHs also showed clear fuel dependence. Previous studies have shown that low- and medium-ring PAHs are more prone to gas-phase or particle-phase oxidation, whereas the formation of different oxygenated products is closely related to the parent precursors and the degree of aromaticity [24,26,27,31].

To characterize toxicity-related changes in target PACs, this study used the QSAR model provided by ADMETlab 2.0 to evaluate the measured pPAHs and oPAHs for which carcinogenicity parameters were available (Figure 5) [32]. In Figure 5, the stacked bars show the absolute contributions of pPAH ring groups and oPAH categories to the QSAR-derived carcinogenicity indicator, whereas the ring charts show their relative contribution structures in Fresh and Aged samples. In both plot types, different colors distinguish the pPAH ring groups and oPAH categories. The results showed that the overall QSAR-derived carcinogenicity indicator of fresh-emission samples was 109.94 and decreased to 59.51 after aging, corresponding to an overall decline of 46%. This change was mainly driven by the decline in the toxicity-related contribution of pPAHs, with the 2–4 rings group decreasing from 63.85 to 25.95 and the 5–6 rings group decreasing from 37.74 to 22.35. By comparison, the absolute contributions of different oPAHs categories changed little, although their relative roles in the total toxicity-related indicator increased as the pPAH contribution declined.

This result was directionally consistent with the compositional evolution shown in Figure 4. After aging, the total amount of pPAHs generally decreased, especially because the reduction in low- and medium-ring parent PAHs was more pronounced; consequently, the decline in the total carcinogenicity indicator was first reflected in the attenuation of the pPAH contribution. At the same time, the toxicity-related contribution profile, which was dominated by pPAHs in fresh emissions, shifted after aging: the combined contribution of the 2–4 rings and 5–6 rings groups decreased from 92% to 81%, whereas the relative

weights of ANTQ, BANO, and Other in the residual toxicity-related indicator increased simultaneously. Previous studies have likewise pointed out that evaluations based only on the traditional 16 EPA priority PAHs do not fully capture aging-induced changes in the contribution structure of toxicity-related indicators [27,31].

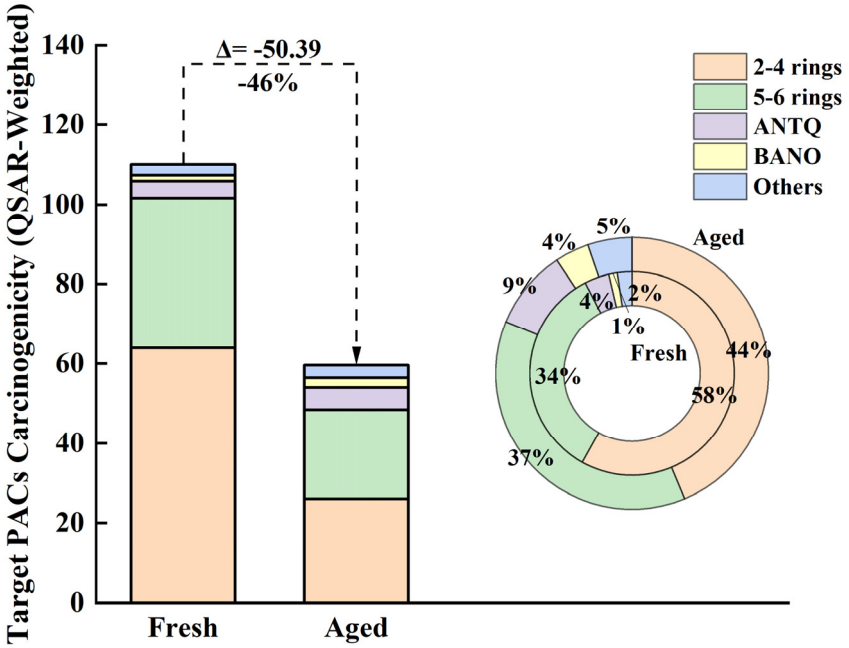

Figure 5. Overall QSAR-derived carcinogenicity of particulate target PACs in fresh emissions and after atmospheric aging, and the corresponding changes in contribution structure. In the ring chart, the inner and outer rings represent Fresh and Aged samples, respectively. Percentages are rounded to the nearest whole number; therefore, the displayed values may not sum exactly to 100%.

As a supplementary comparison, the carcinogenicity of the 16 pPAHs was further evaluated using the benzo[a]pyrene equivalent (BaPeq) method. The total BaPeq of fresh-emission samples decreased from 14.51 to 8.38 mg/kg fuel after aging, showing the same direction of change as the QSAR results. Although the two methods differ in their coefficient sources and numerical scales, both indicate a decrease in the overall potential carcinogenicity indicator of particulate target PACs after aging. Meanwhile, the QSAR results, which include oPAHs, further suggest that the contribution structure of the residual toxicity-related indicator had undergone substantial redistribution. Therefore, toxicity-related characterization of residential solid fuel emissions should not rely solely on fresh emissions or the total amount of parent PAHs, but should also consider changes in oxidized aromatic compounds and the contribution structure of potential carcinogenicity indicators during atmospheric aging [44–46].

4. Conclusions

In this study, a quartz tube furnace, flue-gas dilution system, and oxidation flow reactor (OFR) were directly coupled, enabling a direct comparison of the evolution of particulate-phase components in residential solid fuel combustion emissions from fresh emissions to simulated atmospheric aging within a unified experimental framework. Using straw, wood, and coal as representative fuels, the effects of fuel type and combustion temperature (500 °C and 800 °C) on the emission characteristics of particulate OC and PACs and on their aging responses were systematically investigated.

The results showed that fuel type and combustion temperature jointly determined the initial emission profiles of particulate pollutants. In the fresh-emission stage, increasing

combustion temperature reduced particulate OC emissions for both biomass and coal, whereas PAC emissions showed opposite temperature responses, increasing for biomass but decreasing for coal. This divergence indicates that the effectiveness of combustion optimization or fuel substitution cannot be evaluated by a single fresh-emission metric because reductions in carbonaceous mass do not necessarily imply parallel reductions in all PAC-related indicators. Simulated atmospheric aging further altered both carbonaceous and aromatic components. Particulate OC generally increased after OFR aging, while parent polycyclic aromatic hydrocarbons (pPAHs) decreased and oxygenated PAHs (oPAHs) became relatively more important. The strongest PAC response was observed for coal burned at 500 °C, where pPAHs decreased from 303.58 ± 157.03 to 110.79 ± 85.53 mg/kg fuel, corresponding to a 64% decrease, whereas oPAHs increased from 4.91 ± 3.58 to 11.16 ± 1.67 mg/kg fuel, corresponding to a 127% increase. Together with the aging response of pyrolyzed carbon (PyC), these results suggest that post-emission aging involves not only the depletion of parent compounds, but also the formation and/or retention of more oxidized particulate components.

The compound-based potential carcinogenicity indicators decreased overall after aging, as indicated by both the quantitative structure–activity relationship (QSAR)-derived and benzo[a]pyrene-equivalent (BaPeq)-based methods. However, the contribution pattern changed: oPAHs accounted for a larger fraction of the QSAR-derived potential carcinogenicity indicator after aging, increasing from 7% to 18%. Therefore, evaluations based only on fresh emissions or parent PAHs can overlook important changes in toxicity-related indicators during atmospheric aging. Because these estimates are based on chemical indicators rather than biological toxicity tests, they should be interpreted as potential carcinogenicity indicators rather than direct evidence of actual health effects.

From an application perspective, current evaluations of the environmental performance of small solid-fuel systems mostly focus on indicators such as PM, CO, device thermal efficiency, oxygen supply conditions, or the effects of fuel modification [47,48]. In addition to considering reductions in fresh particulate matter, OC, and pPAHs, technology screening and fuel and combustion optimization should also consider aging-responsive species and indicators, such as oPAHs, PyC, and the contribution structure of potential carcinogenicity indicators. In particular, low-temperature coal combustion deserves attention because of its strong aging-related PAC transformation, whereas biomass combustion should also be assessed for possible PAC formation under higher-temperature conditions, rather than only by OC or PM reductions. These results can help refine emission evaluation frameworks for cleaner-heating and low-emission technologies.

This study was conducted under controlled laboratory combustion and OFR aging conditions, which improved comparability among fuel and temperature groups but cannot fully represent real-world variability in combustion operation, dilution, humidity, NO_x levels, oxidant exposure, atmospheric transport, and multi-generation aging. In addition, the present toxicity-related analysis was limited to selected particulate PACs and indicator-based calculations. Future studies should combine chamber experiments, field observations, multiple aging conditions, simultaneous gas–particle measurements, and biological assays to further test the atmospheric representativeness and toxicological relevance of the indicators identified here.

Supplementary Materials: The following supporting information can be downloaded at: https://www.mdpi.com/article/10.3390/atmos17060578/s1. Figure S1: Schematic of the combustion–dilution–aging sampling system; Figure S2: Emission factors and chemical compositions of particulate-phase OC, parent PAHs (pPAHs), and oxygenated PAHs (oPAHs) in fresh emissions from the 12 fuels under LIC and HIC conditions; Figure S3: Emission factors and chemical compositions of particulate-phase OC, pPAHs, and oPAHs in aged aerosol samples from the 12 fuels under LIC

and HIC conditions; Figure S4: Carcinogenic toxicity of total PACs estimated using the QSAR model in ADMETlab 2.0 and carcinogenic toxicity of pPAHs calculated using the BaPeq method; Text S1: Combustion–dilution–aging sampling system; Text S2: Fuel selection and combustion simulation; Text S3: OFR operation and estimation of equivalent atmospheric aging time; Text S4: PACs analysis and toxicity-related parameters; Text S5: Quality assurance and quality control (QA/QC); Text S6. Calculation of emission factors using the carbon mass balance method; Table S1: Elemental composition of the 12 fuel samples (%); Table S2: Target pPAHs and oPAHs identified by TD-GC/MS; Table S3: The benzo[a]pyrene toxicity equivalents of pPAHs and the carcinogenic parameters of pPAHs and oPAHs obtained based on the Quantitative Structure-Property Relationship (QSAR) model from ADMETlab 2.0. References [12,33,36,49–54] are cited in the Supplementary Materials.

Author Contributions: Conceptualization, Y.L. (Yuwei Liu), Y.P. and Y.C.; methodology, Y.L. (Yuwei Liu), Y.P. and Y.C.; investigation, Y.L. (Yuwei Liu) and Y.P. and Y.L. (Yanjie Lu); formal analysis, Y.L. (Yuwei Liu) and Y.P. and Y.L. (Yanjie Lu); data curation, Y.L. (Yuwei Liu), Y.P.; writing—original draft preparation, Y.L. (Yuwei Liu) and Y.P.; funding acquisition, Y.C.; project administration, Y.C. All authors have read and agreed to the published version of the manuscript.

Funding: This work was funded by the National Natural Science Foundation of China (Grant NOs. 42192514, 42177086, 42477095).

Institutional Review Board Statement: Not applicable.

Informed Consent Statement: Not applicable.

Data Availability Statement: The data presented in this study are available on request from the corresponding author.

Conflicts of Interest: The authors declare no conflicts of interest.

Abbreviations

The following abbreviations are used in this manuscript:

Aged	OFR-aged sample
ANTQ	Anthraquinone-like oPAHs
BANO	Benz[a]anthrone-like oPAHs
BaPeq	Benzo[a]pyrene equivalent
BrC	Brown carbon
EC	Elemental carbon
EF	Emission factor
EF_{OC}	Organic carbon emission factor
EF_{PACs}	PAC emission factor
EF_{pPAHs}	pPAH emission factor
EF_{oPAHs}	oPAH emission factor
Fresh	Fresh-emission sample
HIC	High initial combustion temperature
LIC	Low initial combustion temperature
OC	Organic carbon
OFR	Oxidation flow reactor
PAM-OFR	Potential aerosol mass oxidation flow reactor
PACs	Polycyclic aromatic compounds
PAHs	Polycyclic aromatic hydrocarbons
pPAHs	Parent polycyclic aromatic hydrocarbons
oPAHs	Oxygenated polycyclic aromatic hydrocarbons
PM	Particulate matter
PyC	Pyrolyzed carbon
QA/QC	Quality assurance/quality control
QSAR	Quantitative structure–activity relationship

SIM	Selected ion monitoring
TD-GC/MS	Thermal desorption–gas chromatography/mass spectrometry
TOR	Thermal/optical reflectance

References

1. Shen, H.; Luo, Z.; Xiong, R.; Liu, X.; Zhang, L.; Li, Y.; Du, W.; Chen, Y.; Cheng, H.; Shen, G.; et al. A Critical Review of Pollutant Emission Factors from Fuel Combustion in Home Stoves. *Environ. Int.* **2021**, *157*, 106841. [CrossRef]
2. Li, Q.; Jiang, J.; Wang, S.; Rumchev, K.; Mead-Hunter, R.; Morawska, L.; Hao, J. Impacts of Household Coal and Biomass Combustion on Indoor and Ambient Air Quality in China: Current Status and Implication. *Sci. Total Environ.* **2017**, *576*, 347–361. [CrossRef]
3. Liao, H.; Tang, X.; Wei, Y.-M. Solid Fuel Use in Rural China and Its Health Effects. *Renew. Sustain. Energy Rev.* **2016**, *60*, 900–908. [CrossRef]
4. Bonjour, S.; Adair-Rohani, H.; Wolf, J.; Bruce, N.G.; Mehta, S.; Prüss-Ustün, A.; Lahiff, M.; Rehfuess, E.A.; Mishra, V.; Smith, K.R. Solid Fuel Use for Household Cooking: Country and Regional Estimates for 1980–2010. *Env. Health Perspect* **2013**, *121*, 784–790. [CrossRef] [PubMed]
5. Chafe, Z.A.; Brauer, M.; Klimont, Z.; Van Dingenen, R.; Mehta, S.; Rao, S.; Riahi, K.; Dentener, F.; Smith, K.R. Household Cooking with Solid Fuels Contributes to Ambient $PM_{2.5}$ Air Pollution and the Burden of Disease. *Env. Health Perspect* **2014**, *122*, 1314–1320. [CrossRef]
6. Andreae, M.O. Emission of Trace Gases and Aerosols from Biomass Burning—An Updated Assessment. *Atmos. Chem. Phys.* **2019**, *19*, 8523–8546. [CrossRef]
7. Shen, G.; Tao, S.; Wang, W.; Yang, Y.; Ding, J.; Xue, M.; Min, Y.; Zhu, C.; Shen, H.; Li, W.; et al. Emission of Oxygenated Polycyclic Aromatic Hydrocarbons from Indoor Solid Fuel Combustion. *Environ. Sci. Technol.* **2011**, *45*, 3459–3465. [CrossRef]
8. Yang, X.; Liu, S.; Xu, Y.; Liu, Y.; Chen, L.; Tang, N.; Hayakawa, K. Emission Factors of Polycyclic and Nitro-Polycyclic Aromatic Hydrocarbons from Residential Combustion of Coal and Crop Residue Pellets. *Environ. Pollut.* **2017**, *231*, 1265–1273. [CrossRef] [PubMed]
9. Zhang, Y.; Shen, Z.; Sun, J.; Zhang, L.; Zhang, B.; Zou, H.; Zhang, T.; Hang Ho, S.S.; Chang, X.; Xu, H.; et al. Parent, Alkylated, Oxygenated and Nitrated Polycyclic Aromatic Hydrocarbons in $PM_{2.5}$ Emitted from Residential Biomass Burning and Coal Combustion: A Novel Database of 14 Heating Scenarios. *Environ. Pollut.* **2021**, *268*, 115881. [CrossRef]
10. Wang, J.; Du, W.; Chen, Y.; Lei, Y.; Chen, L.; Shen, G.; Pan, B.; Tao, S. Nitrated and Oxygenated Polycyclic Aromatic Hydrocarbons Emissions from Solid Fuel Combustion in Rural China: Database of 12 Real-World Scenarios for Residential Cooking and Heating Activities. *Sci. Total Environ.* **2022**, *852*, 158501. [CrossRef]
11. Abdel-Shafy, H.I.; Mansour, M.S.M. A Review on Polycyclic Aromatic Hydrocarbons: Source, Environmental Impact, Effect on Human Health and Remediation. *Egypt. J. Pet.* **2016**, *25*, 107–123. [CrossRef]
12. Wang, J.; Jiang, H.; Chen, Y.; Han, Y.; Cai, J.; Peng, Y.; Feng, Y. Emission Characteristics and Influencing Mechanisms of PAHs and EC from the Combustion of Three Components (Cellulose, Hemicellulose, Lignin) of Biomasses. *Sci. Total Environ.* **2023**, *859*, 160359. [CrossRef]
13. Han, Y.; Chen, Y.; Feng, Y.; Song, W.; Cao, F.; Zhang, Y.; Li, Q.; Yang, X.; Chen, J. Different Formation Mechanisms of PAH during Wood and Coal Combustion under Different Temperatures. *Atmos. Environ.* **2020**, *222*, 117084. [CrossRef]
14. Akagi, S.K.; Yokelson, R.J.; Wiedinmyer, C.; Alvarado, M.J.; Reid, J.S.; Karl, T.; Crounse, J.D.; Wennberg, P.O. Emission Factors for Open and Domestic Biomass Burning for Use in Atmospheric Models. *Atmos. Chem. Phys.* **2011**, *11*, 4039–4072. [CrossRef]
15. Tian, J.; Ni, H.; Cao, J.; Han, Y.; Wang, Q.; Wang, X.; Chen, L.W.A.; Chow, J.C.; Watson, J.G.; Wei, C.; et al. Characteristics of Carbonaceous Particles from Residential Coal Combustion and Agricultural Biomass Burning in China. *Atmos. Pollut. Res.* **2017**, *8*, 521–527. [CrossRef]
16. Zhao, X.; Yang, F.; Li, Z.; Tan, H. Formation and Emission Characteristics of PAHs during Pyrolysis and Combustion of Coal and Biomass. *Fuel* **2024**, *378*, 132935. [CrossRef]
17. Grieshop, A.P.; Donahue, N.M.; Robinson, A.L. Laboratory Investigation of Photochemical Oxidation of Organic Aerosol from Wood Fires 2: Analysis of Aerosol Mass Spectrometer Data. *Atmos. Chem. Phys.* **2009**, *9*, 2227–2240. [CrossRef]
18. Hodshire, A.L.; Akherati, A.; Alvarado, M.J.; Brown-Steiner, B.; Jathar, S.H.; Jimenez, J.L.; Kreidenweis, S.M.; Lonsdale, C.R.; Onasch, T.B.; Ortega, A.M.; et al. Aging Effects on Biomass Burning Aerosol Mass and Composition: A Critical Review of Field and Laboratory Studies. *Environ. Sci. Technol.* **2019**, *53*, 10007–10022. [CrossRef]
19. Li, C.; Ma, Z.; Chen, J.; Wang, X.; Ye, X.; Wang, L.; Yang, X.; Kan, H.; Donaldson, D.J.; Mellouki, A. Evolution of Biomass Burning Smoke Particles in the Dark. *Atmos. Environ.* **2015**, *120*, 244–252. [CrossRef]
20. Yazdani, A.; Dudani, N.; Takahama, S.; Bertrand, A.; Prévôt, A.S.H.; El Haddad, I.; Dillner, A.M. Characterization of Primary and Aged Wood Burning and Coal Combustion Organic Aerosols in an Environmental Chamber and Its Implications for Atmospheric Aerosols. *Atmos. Chem. Phys.* **2021**, *21*, 10273–10293. [CrossRef]

21. Zhang, Y.; Sun, J.; Zou, H.; Zhang, B.; Yang, D.; Wang, Q.; Li, J.; Qu, L.; Ho, S.S.H.; Cao, J.; et al. Photochemical Aging Process on $PM_{2.5}$ Bound PAHs Emission from Solid Fuel Combustion in Traditional and Improved Stoves. *Atmos. Res.* **2021**, *263*, 105807. [CrossRef]
22. Reece, S.M.; Sinha, A.; Grieshop, A.P. Primary and Photochemically Aged Aerosol Emissions from Biomass Cookstoves: Chemical and Physical Characterization. *Environ. Sci. Technol.* **2017**, *51*, 9379–9390. [CrossRef]
23. Hennigan, C.J.; Miracolo, M.A.; Engelhart, G.J.; May, A.A.; Presto, A.A.; Lee, T.; Sullivan, A.P.; McMeeking, G.R.; Coe, H.; Wold, C.E.; et al. Chemical and Physical Transformations of Organic Aerosol from the Photo-Oxidation of Open Biomass Burning Emissions in an Environmental Chamber. *Atmos. Chem. Phys.* **2011**, *11*, 7669–7686. [CrossRef]
24. Hartikainen, A.; Tiitta, P.; Ihalainen, M.; Yli-Pirilä, P.; Orasche, J.; Czech, H.; Kortelainen, M.; Lamberg, H.; Suhonen, H.; Koponen, H.; et al. Photochemical Transformation of Residential Wood Combustion Emissions: Dependence of Organic Aerosol Composition on OH Exposure. *Atmos. Chem. Phys.* **2020**, *20*, 6357–6378. [CrossRef]
25. Fang, Z.; Li, C.; He, Q.; Czech, H.; Gröger, T.; Zeng, J.; Fang, H.; Xiao, S.; Pardo, M.; Hartner, E.; et al. Secondary Organic Aerosols Produced from Photochemical Oxidation of Secondarily Evaporated Biomass Burning Organic Gases: Chemical Composition, Toxicity, Optical Properties, and Climate Effect. *Environ. Int.* **2021**, *157*, 106801. [CrossRef]
26. Zhou, S.; Hwang, B.C.H.; Lakey, P.S.J.; Zuend, A.; Abbatt, J.P.D.; Shiraiwa, M. Multiphase Reactivity of Polycyclic Aromatic Hydrocarbons Is Driven by Phase Separation and Diffusion Limitations. *Proc. Natl. Acad. Sci. USA* **2019**, *116*, 11658–11663. [CrossRef]
27. Sengupta, D.; Samburova, V.; Bhattarai, C.; Moosmüller, H.; Khlystov, A. Emission Factors for Polycyclic Aromatic Hydrocarbons from Laboratory Biomass-Burning and Their Chemical Transformations during Aging in an Oxidation Flow Reactor. *Sci. Total Environ.* **2023**, *870*, 161857. [CrossRef]
28. Ray, D.; Ghosh, S.K.; Raha, S. Impacts of Photochemical Ageing on the Half-Lives and Diagnostic Ratio of Polycyclic Aromatic Hydrocarbons Intrinsic to $PM_{2.5}$ Collected from 'Real-World' like Combustion Events of Wood and Rice Straw Burning. *J. Hazard. Mater.* **2019**, *366*, 10–15. [CrossRef]
29. Miersch, T.; Czech, H.; Hartikainen, A.; Ihalainen, M.; Orasche, J.; Abbaszade, G.; Tissari, J.; Streibel, T.; Jokiniemi, J.; Sippula, O.; et al. Impact of Photochemical Ageing on Polycyclic Aromatic Hydrocarbons (PAH) and Oxygenated PAH (Oxy-PAH/OH-PAH) in Logwood Stove Emissions. *Sci. Total Environ.* **2019**, *686*, 382–392. [CrossRef]
30. Han, Y.; Cai, J.; Chen, Y.; Zhang, Y.; Jin, L.N.; Chen, T.; Li, J.; Zhang, G.; Chen, J. Concurrent Formation of Low-Maturity EC and BrC in Biomass and Coal Burning: O-PAH as a Precursor. *Environ. Sci. Technol.* **2025**, *59*, 12083–12095. [CrossRef]
31. Cao, F.; Feng, X.; Chen, Y.; Jiang, H.; Han, Y.; Chen, T.; Shang, Y.; Li, D.; Zhang, Q.; Ma, H.; et al. Oxygenated Aromatic Compounds as Dominant Contributors to the Oxidative Potential of $PM_{2.5}$ Emitted from Biomass Burning and Coal Combustion. *J. Hazard. Mater.* **2025**, *498*, 139902. [CrossRef]
32. Xiong, G.; Wu, Z.; Yi, J.; Fu, L.; Yang, Z.; Hsieh, C.; Yin, M.; Zeng, X.; Wu, C.; Lu, A.; et al. ADMETlab 2.0: An Integrated Online Platform for Accurate and Comprehensive Predictions of ADMET Properties. *Nucleic Acids Res.* **2021**, *49*, W5–W14. [CrossRef]
33. Han, Y.; Chen, Y.; Ahmad, S.; Feng, Y.; Zhang, F.; Song, W.; Cao, F.; Zhang, Y.; Yang, X.; Li, J.; et al. High Time- and Size-Resolved Measurements of PM and Chemical Composition from Coal Combustion: Implications for the EC Formation Process. *Environ. Sci. Technol.* **2018**, *52*, 6676–6685. [CrossRef]
34. Louis, C.; Liu, Y.; Martinet, S.; D'Anna, B.; Valiente, A.M.; Boreave, A.; R'Mili, B.; Tassel, P.; Perret, P.; André, M. Dilution Effects on Ultrafine Particle Emissions from Euro 5 and Euro 6 Diesel and Gasoline Vehicles. *Atmos. Environ.* **2017**, *169*, 80–88. [CrossRef]
35. Zheng, S.; Kong, S.; Yan, Q.; Zhang, Y.; Zheng, H.; Chen, K.; Yin, Y.; Liu, D.; Li, W. Impact of Dilution Ratio and Burning Conditions on the Number Size Distribution and Size-Dependent Mixing State of Primary Particles from Domestic Solid Fuel Burning. *Environ. Sci. Technol. Lett.* **2022**, *9*, 611–617. [CrossRef]
36. Peng, Z.; Day, D.A.; Stark, H.; Li, R.; Lee-Taylor, J.; Palm, B.B.; Brune, W.H.; Jimenez, J.L. HO_x Radical Chemistry in Oxidation Flow Reactors with Low-Pressure Mercury Lamps Systematically Examined by Modeling. *Atmos. Meas. Tech.* **2015**, *8*, 4863–4890. [CrossRef]
37. Rowe, J.P.; Lambe, A.T.; Brune, W.H. Technical Note: Effect of Varying the λ = 185 and 254 Nm Photon Flux Ratio on Radical Generation in Oxidation Flow Reactors. *Atmos. Chem. Phys.* **2020**, *20*, 13417–13424. [CrossRef]
38. Nisbet, I.C.T.; LaGoy, P.K. Toxic Equivalency Factors (TEFs) for Polycyclic Aromatic Hydrocarbons (PAHs). *Regul. Toxicol. Pharmacol.* **1992**, *16*, 290–300. [CrossRef]
39. U.S. Environmental Protection Agency. *Other Test Method 48 (OTM-48): Emission Factor Determination by the Carbon Balance Method—Method to Quantify Emissions from Open Area Sources*; U.S. Environmental Protection Agency, Office of Air Quality Planning and Standards: Durham, NC, USA, 2022.
40. Czaplicka, M.; Cieślik, E.; Komosiński, B.; Rachwał, T. Emission Factors for Biofuels and Coal Combustion in a Domestic Boiler of 18 kW. *Atmosphere* **2019**, *10*, 771. [CrossRef]

41. Zhang, H.; Zhang, X.; Wang, Y.; Bai, P.; Hayakawa, K.; Zhang, L.; Tang, N. Characteristics and Influencing Factors of Polycyclic Aromatic Hydrocarbons Emitted from Open Burning and Stove Burning of Biomass: A Brief Review. *IJERPH* **2022**, *19*, 3944. [CrossRef]
42. Xu, W.; Li, Z.; Zhang, Z.; Li, J.; Karnezi, E.; Lambe, A.T.; Zhou, W.; Sun, J.; Du, A.; Li, Y.; et al. Changes in Physicochemical Properties of Organic Aerosol During Photochemical Aging of Cooking and Burning Emissions. *JGR Atmos.* **2023**, *128*, e2022JD037911. [CrossRef]
43. Sinha, A.; George, I.; Holder, A.; Preston, W.; Hays, M.; Grieshop, A.P. Development of Volatility Distributions for Organic Matter in Biomass Burning Emissions. *Environ. Sci. Atmos.* **2023**, *3*, 11–23. [CrossRef]
44. Wang, S.; Gallimore, P.J.; Liu-Kang, C.; Yeung, K.; Campbell, S.J.; Utinger, B.; Liu, T.; Peng, H.; Kalberer, M.; Chan, A.W.H.; et al. Dynamic Wood Smoke Aerosol Toxicity during Oxidative Atmospheric Aging. *Environ. Sci. Technol.* **2023**, *57*, 1246–1256. [CrossRef]
45. Wong, J.P.S.; Tsagkaraki, M.; Tsiodra, I.; Mihalopoulos, N.; Violaki, K.; Kanakidou, M.; Sciare, J.; Nenes, A.; Weber, R.J. Effects of Atmospheric Processing on the Oxidative Potential of Biomass Burning Organic Aerosols. *Environ. Sci. Technol.* **2019**, *53*, 6747–6756. [CrossRef]
46. Kim, Y.H.; Sinha, A.; George, I.J.; DeMarini, D.M.; Grieshop, A.P.; Gilmour, M.I. Toxicity of Fresh and Aged Anthropogenic Smoke Particles Emitted from Different Burning Conditions. *Sci. Total Environ.* **2023**, *892*, 164778. [CrossRef]
47. Delcourt, F.; Izerroukyene, A.; Méresse, D.; Uystepruyst, D.; Beaubert, F.; Morin, C. Experimental Study of Pollutant Emissions from Biomass Combustion and Modeling of PM Transportation. *Energies* **2024**, *17*, 2586. [CrossRef]
48. Dragutinović, N.; Höfer, I.; Kaltschmitt, M. Fuel Improvement Measures for Particulate Matter Emission Reduction during Corn Cob Combustion. *Energies* **2021**, *14*, 4548. [CrossRef]
49. Li, K.; Liggio, J.; Lee, P.; Han, C.; Liu, Q.; Li, S.-M. Secondary Organic Aerosol Formation from α-Pinene, Alkanes, and Oil-Sands-Related Precursors in a New Oxidation Flow Reactor. *Atmos. Chem. Phys.* **2019**, *19*, 9715–9731. [CrossRef]
50. Simonen, P.; Saukko, E.; Karjalainen, P.; Timonen, H.; Bloss, M.; Aakko-Saksa, P.; Rönkkö, T.; Keskinen, J.; Dal Maso, M. A New Oxidation Flow Reactor for Measuring Secondary Aerosol Formation of Rapidly Changing Emission Sources. *Atmos. Meas. Tech.* **2017**, *10*, 1519–1537. [CrossRef]
51. Nyström, R.; Lindgren, R.; Avagyan, R.; Westerholm, R.; Lundstedt, S.; Boman, C. Influence of Wood Species and Burning Conditions on Particle Emission Characteristics in a Residential Wood Stove. *Energy Fuels* **2017**, *31*, 5514–5524. [CrossRef]
52. Sun, J.; Zhi, G.; Jin, W.; Chen, Y.; Shen, G.; Tian, C.; Zhang, Y.; Zong, Z.; Cheng, M.; Zhang, X.; et al. Emission Factors of Organic Carbon and Elemental Carbon for Residential Coal and Biomass Fuels in China—A New Database for 39 Fuel-Stove Combinations. *Atmos. Environ.* **2018**, *190*, 241–248. [CrossRef]
53. Cao, W.; Li, J.; Martí-Rosselló, T.; Zhang, X. Experimental Study on the Ignition Characteristics of Cellulose, Hemicellulose, Lignin and Their Mixtures. *J. Energy Inst.* **2019**, *92*, 1303–1312. [CrossRef]
54. Han, Y.; Chen, Y.; Feng, Y.; Shang, Y.; Li, J.; Li, Q.; Chen, J. Fuel Aromaticity Promotes Low-Temperature Nucleation Processes of Elemental Carbon from Biomass and Coal Combustion. *Environ. Sci. Technol.* **2021**, *55*, 2532–2540. [CrossRef]